Polymer 226 (2021) 123799

Contents lists available at ScienceDirect

Polymer

journal homepage: www.elsevier.com/locate/polymer

The effect of copolymerization of cyclic dioxolane moieties on polyamide properties

Aleksandra A. Wróblewska [a,b], Jules A.W. Harings [a], Peter Adriaensens [c], Stefaan M. A. De Wildeman [a], Katrien V. Bernaerts [a,*]

[a] Faculty of Science and Engineering, Biobased Materials, Maastricht University, P.O. Box 616, 6200MD, Maastricht, the Netherlands
[b] Flemish Institute for Technological Research (Vito N.V.), Boeretang 200, 2400 Mol, Belgium
[c] Analytical and Circular Chemistry, Institute for Materials Research, Hasselt University, Agoralaan1 Building D, B-3590, Diepenbeek, Belgium

ARTICLE INFO

Keywords:
Galactaric acid
Biacetalized
DFT
Temperature dependent-FTIR
Solid-state NMR
DMTA
Potential energy surface
Polyamides
Bio-based

ABSTRACT

Upon copolymerization of carbohydrate-based cyclic moieties, they offer a variety of new functionalities and a convenient way to modify the properties of the material. Structurally the electronegative sites present in the cyclic structures have a major influence on hydrogen bonding. In this study the consequences of the incorporation of 2,3:4,5-di-*O*-methylene-galactarate (GalXH) and 2,3:4,5-di-*O*-isopropylidene-galactarate (GalXMe) cyclic moieties in aliphatic polyamides are investigated by FT-IR and solid state NMR and a correlation is made with the thermomechanical properties and crystallinity of the copolyamides. The analysis is complemented by the theoretical calculations, which suggest that the amide proton of such polyamides tends to form hydrogen bonds with the acetal oxygen of neighboring GalX (intramolecular) and therefore prevents the interchain hydrogen bonding, resulting in decreased hydrogen bonding density. Despite the conformational rigidity of the GalX comonomers, the decrease in interchain hydrogen bonding leads to a counter intuitive decrease in glass transition temperature with increasing mole percentage GalX comonomer. As suspected the copolymerization of GalX with aliphatic monomers suppresses the crystallinity which is more pronounced for bulkier monomers.

1. Introduction

Biomass is a very attractive source of monomers mostly due to the wide-spread availability and the variety of molecules, which can be obtained therefrom [1]. Beet root pulp is a waste product from food industry (a second generation biomass), which makes it more competitive towards fossil-based chemicals and fuels [2,3]. Examples of biomass-derived monomers are alcohols and acids based on isohexides or biacetalized carbohydrate derivatives like acetals of galactarate (GalX) [4–18] (Fig. 1, top).

GalX is a molecule obtained by extraction and chemical modification of molecules obtained from sugar beet pulp [19,20] and possesses two dioxolane rings or substituted dioxolane rings connected by a carbon-carbon linkage, which contribute to very specific properties of the molecule and polymers therefrom. The GalX molecule has 4 chiral carbons; however it has a *meso* configuration which makes it optically not active due to its exact mirror image. Due to the rigidity of the dioxolane rings GalX can contribute to improved thermal properties like increased glass transition temperature and increased melting temperature [7,15,17,21]. The bulky character of ring structures incorporated into linear polyesters or polyamides can highly hamper close chain packing which is characteristic for semi-crystalline materials, challenging crystallization and lowering the melting temperature [22]. Indeed, upon the incorporation of GalX into polyamides (based on DSC [15,23]) or polyesters (WAXD analysis of crystals [21,22]) the crystallinity of those polymers is highly suppressed and drops to almost zero already at 30% of these moieties in the copolymer. In consequence of this, the GalX contribution has predominant influences on the mechanical properties of polymers therefrom and alters its appearance to transparent.

Available literature reports show that the exact structure of those biacetalized moieties controls a lot of properties starting from the hydrolytic or thermal stability [15,24–28] to even solubility [29]. The important factors are on one hand the structure of the acetal protection (methylene or i-propylidene acetal) and on the other hand the ring structure and orientation e.g. 6-membered 1,3-dioxane fused rings of

* Corresponding author.
E-mail address: katrien.bernaerts@maastrichtuniversity.nl (K.V. Bernaerts).

https://doi.org/10.1016/j.polymer.2021.123799
Received 18 February 2021; Received in revised form 12 April 2021; Accepted 20 April 2021
Available online 24 April 2021

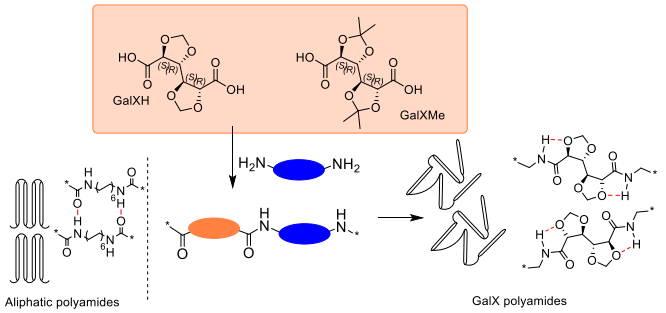

Fig. 1. General scheme representing a typical hydrogen bonding network present in aliphatic polyamides and the possible hydrogen bonding occurring in GalX-based polyamides.

biacetalized D-mannaric (ManX) and biacetalized D-glucaric acid (GluX) [30] moieties give different RESULTS than GalX, a molecule with two 5-membered 1,3-dioxolane rings which are separated by a *C*–C bond.

Despite that the influence of cyclic acetal moieties on the properties of polymers therefrom is already described, the exact interactions which lead to it, are still not fully understood. Especially with regard to polyamides, whose properties are strongly determined by the inter- and intrachain hydrogen bonding, which can be significantly disrupted by the presence of additional electronegative atoms in the structure and the bulkiness of the cyclic moieties [31–34]. Moreover, biacetalized carbohydrate-based polyamides are not fully investigated and far most of the studies published through the last couple of decades focused on polyesters and copolyesters or polyurethanes [6,35,36] rather than polyamides. The research conducted on polyamides included rather synthetic methods in solution [37] or in melt [15–18,38,39]. In contrast, isohexide-based polyamides are much broader investigated [11,14,40,41], also with regard to the influence on the crystalline domains as well as the interactions with other moieties in the polymer, including theoretical calculations and conformational analysis.

In order to define the ultimate performance of these new bio-based polymers, and consequently also the field of application, we report the in-depth investigation of the relation between GalX moieties and other molecular fragments of polyamides. In order to establish the connection, homopolyamides and copolyamides were studied by FT-IR, temperature dependent FT-IR, Dynamic Mechanical Thermal Analysis (DMTA) and ^{13}C solid state Cross-Polarization/Magic Angle Spinning (CP/MAS) NMR in combination with Density Functional Theory calculations (DFT). The combination of the abovementioned techniques already in the past proved to be very efficient in the investigation of the properties of interest for this study, like solid-state NMR or FT-IR for hydrogen bonding [42–44], DMTA for the thermomechanical behavior, or DFT for conformational analysis [45]. Two different GalX monomers were investigated, GalXH and GalXMe, to understand their influence and specific conformational dynamics on the amplitude of thermomechanical changes.

2. Materials and methods

Materials. 2,3:4,5-di-*O*-isopropylidene-galactaric acid >99%, and 2,3:4,5-*O*-dimethylene-galactaric acid >99%, diethyl 2,3:4,5-di-*O*-isopropylidene-galactarate >99%, diethyl 2,3:4,5-di-*O*-methylene-galactarate>99%, were supplied by Royal Cosun. 1,6-hexamethylenediamine (C6-HMDA) 98%, 1,12-dodecanediamine (C12-DDDA) 98%, decanedioic acid (C10) 98%, sodium hypophosphite monohydrate >99% ($NaHPO_3{\cdot}H_2O$) were purchased from Sigma-Aldrich and used as supplied. 1,1,1,3,3,3-hexafluoro-2-propanol (HFIP) was purchased from Acros Organics. Acetone was purchased from Biosolve.

Synthesis of homopolyamides poly (hexamethylene-2,3:4,5-*O*-isopropylidene-galactaramide and poly (hexamethylene-2,3:4,5-*O*-methylene-galactaramide was conducted according to the procedure described by Wróblewska et al. [15].

Synthesis of copolyamides Poly (1,6-diaminohexane-1,12-dodecanedioate)-*co*-poly (1,6-diaminohexane-2,3:4,5-*O*-isopropylidene-galactarate) and poly (1,6-diaminohexane-1,12-dodecanedioate)-*co*-(1,6-diaminohexane-2,3:4,5-*O*-methylene-galactarate) was conducted according to the procedure described by Wróblewska et al. [18].

2.1. Characterization

Potential energy surfaces (PES) were calculated using the density functional theory (DFT) method with diffusion functions on heavy atoms and polarization functions on hydrogen using the B3-LYP/6-31G (d,p) basis set with Gaussian 09 and GaussView 05 as software package [46]. Conformational analysis was performed by scanning two dihedral angles i.e. Φ and Ψ from 0° to 180° with optimization and frequency calculations in each step. The geometries in all located minima were additionally re-evaluated using the same level of theory to achieve correct angles and interatomic distances. Potential energy values were normalized towards the global minimum and expressed in kcal/mol. The population of conformers was calculated using Boltzman's formula describing the ratio of populations of two states i and j: $N_j/N_i = EXP(-(\varepsilon_j-\varepsilon_i)/kT))$, ε – energy of conformer in miliHartree (mHa), kT∼1mHa at room temperature [47]. The NMR simulation was performed for minima with a population above 1%. The structures were further optimized with the 6-311G+(d,p) basis set. The NMR shielding tensors were computed with the Gauge-Independent Atomic Orbital (GIAO) method. The calculations were conducted on an Intel® Xeon® workstation equipped with CPU E5-2650 v4, 2.2 GHz and 32 GB ram memory.

Molecular weights of polyamides were determined via Gel Permeation Chromatography (GPC). The polymers were dissolved in HFIP with 0,019% NaTFA salt. The sample for GPC measurement was prepared by dissolving 5.0 mg of the polymer in 1.5 mL of the solvent. The solutions were filtered over a 0.2 μm PTFE syringe filter before injection. The GPC apparatus was calibrated with poly (methyl methacrylate) standards. Two PFG combination medium microcolumns with 7 μm particle size (4.6 × 250 mm, separation range 100–1.000.000 Da) and precolumn PFG combination medium with 7 μm particle size (4.6 × 30 mm) were used in order to determine molecular weight and dispersities making use of a Refractive Index detector (RI).

Copolyamide films were prepared by dissolving around 1 g of a polymer in 10 mL HFIP. Upon full dissolution the mixture was placed in Teflon coated crystallization dishes and left overnight under the fumehood for HFIP to evaporate. The Teflon Petri dish was covered with another Petri dish to ensure slow evaporation of the solvent. This procedure resulted in a thin polyamide film.

The thermal profiles were recorded using differential scanning calorimetry (DSC) on a Netzsch Polyma 2014 DSC. DSC data were obtained from about 2 to 5 mg of polymer film at heating/cooling rates of 1 °C/min^{-1} and 10 °C/min under a nitrogen flow of 20 mL min^{-1}. Indium, zinc, tin and bismuth were used as standards for temperature and enthalpy calibration. DSC heating and cooling cycles were performed from 25 to 250 °C. The reported melting temperatures and the enthalpy values of polyamide films correspond to the first heating cycle.

Infrared spectroscopy (FTIR) and temperature – dependent infrared spectroscopy (td-FTIR) were performed on a PerkinElmer FTIR/NIR spectrometer Frontier with resolution 4 cm^{-1} and 8 accumulations per spectrum. A polyamide powder was melted on the FT-IR crystal and slowly cooled down to room temperature. Subsequently, such a sample was heated from 40 °C to 180 °C with a heating rate of 10 °C/min and spectra were recorded at temperature intervals of 10 °C. The background scan was recorded at 180 °C with 64 accumulations and resolution 4 cm^{-1}. RESULTS were normalized to the stretch vibration of the methylene group at 2920 cm^{-1}. All data were processed using the Spectrum (PerkinElmer) software package and SpectraGryph 1.0.3.

^{13}C Solid state NMR Carbon-13 solid-state CP/MAS (Cross-

Polarization/MagicAngle Spinning) NMR spectra were acquired on a Bruker Avance 400 MHz spectrometer (9.4 T wide bore magnet) equipped with a 4 mm BL4 X/Y/H probe. Magic angle spinning was performed at 13 kHz using ceramic rotors of 4 mm in diameter. The aromatic signal of hexamethylbenzene was used to determine the Hartmann-Hahn condition ($\omega_{1H} = \gamma_H B_{1H} = \gamma_C B_{1C} = \omega_{1C}$) for cross-polarization and to calibrate the carbon chemical shift scale (132.1 ppm). Acquisition parameters used were the following: a spectral width of 50 kHz, a 90° pulse length of 3.6 μs, a spin-lock field for cross-polarization of 50 kHz, a contact time for cross-polarization of 1.5 ms, an acquisition time of 15 ms, a recycle delay time of 5 s and about 12000 accumulations. High power proton dipolar decoupling during the acquisition time was set to 80 kHz.

Dynamic Mechanical Thermal Analysis (DMTA) Tensile bars with 10 mm gauge length and 2 mm gauge width (ISO37, type) were punched from films casted from a HFIP solution and measured in tensile mode using a Mettler Toledo STAR^e DMA1 apparatus under nitrogen atmosphere. The samples were dried at 80 °C under vacuum for 24 h and immediately after exposed to temperature sweeps ranging from −60 to 120 °C employing a heating rate of 10 °C/min, a frequency of 1 Hz, 10 μm amplitude and 1.0 N pre-load.

3. RESULTS and discussion

Structure and synthesis of polyamides. In this study two different polymeric materials are studied: homopolymers containing GalX and 1,12-dodecanediamine (DDDA), and copolymers containing two acid functionalized compounds, GalX and sebacic acid (SA) in different ratio's combined with 1,12-dodecanediamine (DDDA) (Fig. 2, Table 1). The homopolymer PA1 in Table 1 is a polymer, which is fully amorphous, highly transparent and brittle. The second type of material, a series of copolymers, is a semi-crystalline material in which the crystallinity strongly depends on the amount of GalX. The composition of those polymers was elucidated by liquid NMR and Maldi-ToF and is in detail described in our previous publications as well as in the synthetic approach [15,18].

Molecular interactions of amide protons. Polyamides are well-known for their organized crystalline structure which is based on strong hydrogen bonds between H (N–H) and O (C═O) of adjacent amide moieties. These amide motifs can be intra- and interchain in nature, i.e. amide groups belonging to a single chain or different chains (Fig. 3). Next to the unique intrachain/intramolecular hydrogen bonding in the GalX-based polyamides depicted in Fig. 3, it is to be noted that intrachain hydrogen bonding in polyamides may also occur between moieties that are positioned further spaced within the same chain.

Infrared analysis allows to characterize hydrogen bonding, their efficiency as well as the conformation that can be adopted by molecules or locations (in or outside the crystals). Fig. 4 presents the region of the N–H stretching vibration of two GalX polyamides and an aliphatic highly crystalline polymer containing dodecanediamine and sebacic acid PA (DDDA,SA). The latter one shows a peak of the strongly hydrogen bonded N–H vibration (at 3306 cm^{-1}). In aliphatic polyamides weakly hydrogen bonded amide protons occur rarely, but are present in the amorphous phase and prominent at elevated temperature e.g. above the melting point [48] when they can be easily detected by FT-IR spectroscopy. However, in the spectra of GalX homopolyamide it is clearly visible that an additional peak above 3400 cm^{-1} occurs which belongs to weakly hydrogen bonded N–H. The peaks of the investigated GalX polyamides are much broader than for the aliphatic reference PA (DDDA,SA), what is typically associated with increased randomization of its conformers due to weakening of hydrogen bonding [49]. In the comparison of the GalX based polyamides to the reference polyamide PA (DDDA,SA), the most perturbing factor in hydrogen bond formation is the difference between the energy optimized length of sebacic acid and GalX moieties along theoretical crystalline chain segments (12.6 and 7.0 Å respectively, Figure S4), hindering special alignment of hydrogen bonding moieties and crystallization. However, the N–H stretching mode may also be influenced by additional interactions between O (O–*C*–O/acetal) and H (N–H) as sketched in Fig. 4. Due to the close proximity and limited motion of such local intramolecular interactions, the hydrogen bonded NH-stretch vibration will shift to lower wavenumber (3281 cm^1) as witnessed by the FTIR spectrum in Fig. 4. Simultaneously these effects hamper the ability of GalX polymers to

Table 1
Characteristics of homo- and copolyamides from sebacic acid (SA), GalX (GalXH and GalXMe) and 1,12-dodecanediamine (DDDA).

Entry	Series	Composition[a]	M_n[b] [kg/mol]	$Đ$[b]	T_g[c] [°C]	T_m[c] [°C]	ΔH_m[c] [J/g]
PA1	Reference	$DDDA_{93}$/SA_{100}	11.0	2.7	78	192/200	67
*co*PA2	Series GalXH	$GalXH_9$/$DDDA_{101}$/SA_{91}	9.0	2.4	70	184/195	76
*co*PA3		$GalXH_{27}$/$DDDA_{105}$/SA_{73}	12.0	2.6	60	180/187	54
*co*PA4		$GalXH_{49}$/$DDDA_{105}$/SA_{51}	16.0	2.7	46	170/180	23
PA5		$DDDA_{102}$/$GalXH_{100}$	31.0	5.7	49*	189	29
*co*PA6	Series GalXMe	$GalXMe_8$/$DDDA_{103}$/SA_{92}	14.0	4.0	71	185/192	60
*co*PA7		$GalXMe_{24}$/$DDDA_{105}$/SA_{76}	21.0	6.0	56	171	31
*co*PA8		$GalXMe_{44}$/$DDDA_{105}$/SA_{56}	31.0	5.9	51	146	11
PA9		$DDDA_{102}$/$GalXMe_{100}$	21.0	2.0	51*	–	–

[a] Composition of the copolymer as determined by NMR, subscripts represent molar % of acid functionalized monomers (GalX and SA) and amine functionalized monomer (DDDA).
[b] Determined by GPC in HFIP with PMMA standards.
[c] Determined on films casted from HFIP solution via DMTA with a heating rate 10 °C/min or *via DSC from the 2nd heating cycle with a heating rate 10 °C/min.

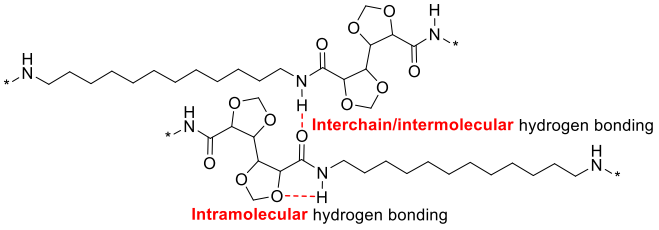

Fig. 3. The definition of interchain and intramolecular hydrogen bonding which can be formed in the GalX-based polyamides.

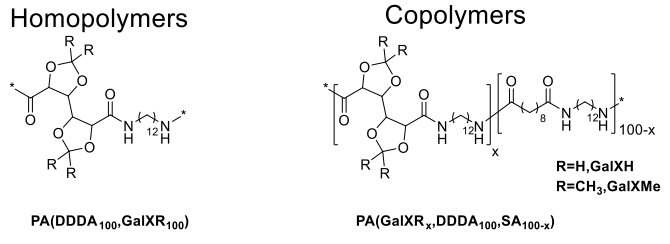

Fig. 2. (Co)Polyamides studied in this work. Subscripts represent molar ratio's of monomers.

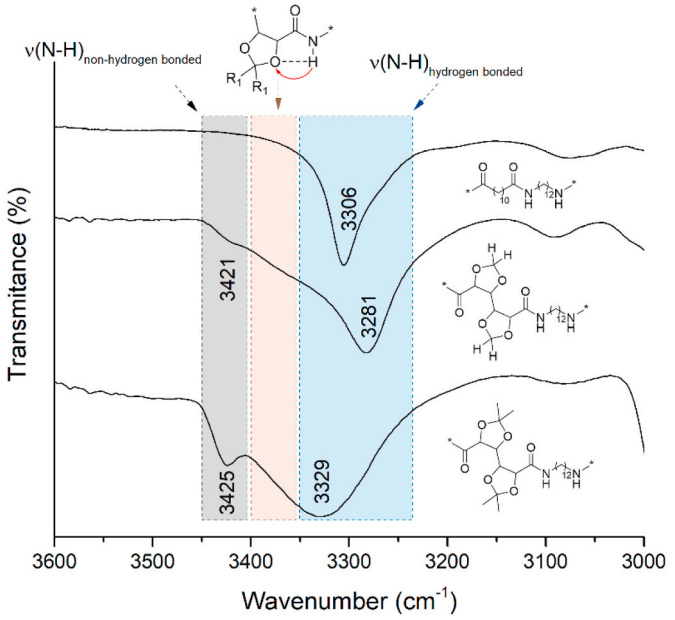

Fig. 4. FT-IR spectra showing the stretching vibration of N–H (3600–3000 cm^{-1}) in homopolyamides PA (DDDA,SA) PA1 top, PA (DDDA, GalXH) PA5 middle and PA (DDDA, GalXMe) PA9 bottom.

form typical amide-amide hydrogen bonding and therefore hampering crystallization, supporting the presence of a second, broad (i.e. more mobile and less efficiently hydrogen bonded) NH stretch band at higher wavenumber, 3425 cm^{-1}. This phenomenon is much more pronounced for GalXMe due to an additional steric effect of the bulkier isopropylidene acetal, hampering amide-amide hydrogen bonding even more. Furthermore, the broadness of the hydrogen bonded NH stretch mode at relatively high wavenumber, namely 3329 cm^{-1}, suggest that also intramolecular hydrogen bonding between the O (O–*C*–O/acetal) and H (N–H) is hampered.

GalX amide conformations by the formation of intramolecular hydrogen bonds between H(N–H)$_{GalX}$ and acetal. In order to elucidate the structure of GalX in polyamides the potential energy surfaces (PES) were calculated for both GalX esters and GalX amides. The difference in those surfaces provides information on how the presence of additional amide hydrogens (N–H) influences the conformation of the molecule. The energy surfaces were obtained by a relaxed scan along two dihedrals with redundant coordinates (Fig. 5). The first scanned coordinate is the dihedral angle between two acetal rings Ψ and the second scanned coordinate is the dihedral angle between ring and carbonyl Φ. The input files related to the performed calculations can be found in section 1 and section 2 of the Supporting Information.

The scan revealed that both GalX molecules have four minima in the investigated range of dihedral angles. The minima A and C correspond to the 40–100° angle Ψ between the two acetal rings and minima B and D to angle Ψ around 180°. Additionally, two minima (A and B) have the dihedral Φ between the carbonyl group and the acetal ring around 180° and the two other (C and D) around 40-0°. The A structure represents a global minimum whereas structures B, C and D are the local minima. In all presented structures amide hydrogen atom H_{30}/H_{26} is located within a hydrogen-bond-formation distance to an oxygen atom within the molecule. The distances between those two atoms are presented in Table 2. It is clear that both investigated GalX can form similar structures; however, the distribution of conformers in the sample varies significantly. Based on the Boltzmann's formula, GalXH appears to have more stable conformers in the sample and the difference in energy between particular structures is lower than for GalXMe as supported by the respective wavenumbers of the hydrogen bonded NH stretch bands in FTIR, 3281 and 3329 cm^{-1} respectively. The rotational energy required for the transformation of one structure to another is much lower in case of GalXH and increases significantly for GalXMe, most probably due to the sterical hindrance provided by the methyl groups on the isopropylidene acetal. Simultaneously, the presence of those additional groups influences the values of both dihedral angles of the optimized structures. All registered minima have a distance between the N–H proton and the oxygen within hydrogen bond distance. The location of those four minima in this position is of high importance since it allows drawing the conclusion that the structures of the GalX amide are stabilized by the formation of intramolecular hydrogen bonds with one of the acetal oxygen atoms (see Table 2 for the distances between proton (NH) and oxygen (O)). If we translate this to a macromolecular system, like polyamide, this observation reveals lower affinity of amide protons to form interchain amide-amide hydrogen bonding and shows that

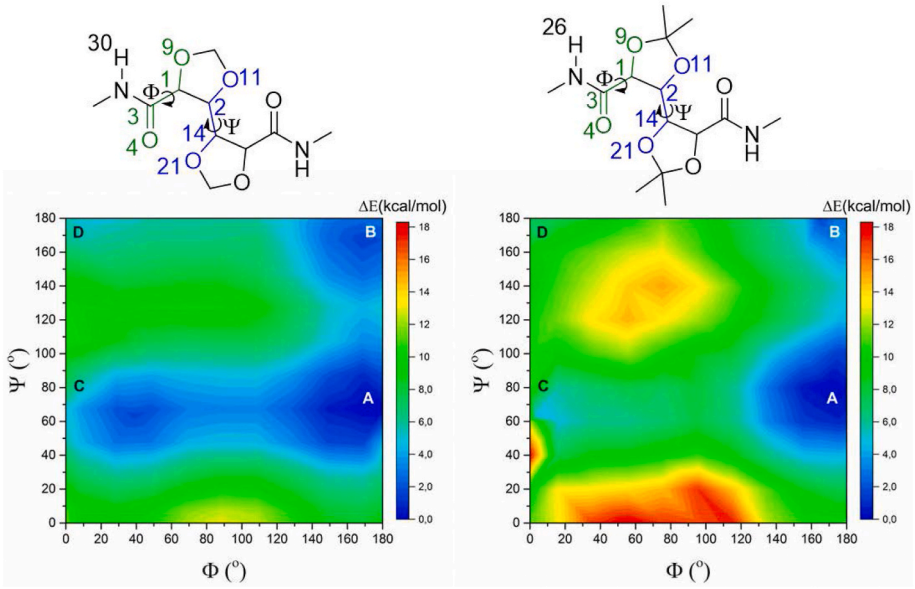

Fig. 5. PES obtained by energy calculation and optimization of two GalX–NH–CH_3 molecules: GalXH–NH–CH_3 (left) and GalXMe–NH–CH_3 (right). The surfaces were calculated along two scanned dihedrals Φ (atoms O_9–C_1–C_3–O_4) and Ψ (atoms O_{11}–C_2–C_{14}–O_{21}) from 0° to 180°. Four located minima are labeled as A, B, C and D. The A structure is corresponding to the global minimum and B, C, D to local minima.

Table 2
The calculated values of scanned coordinates for optimized structures of GalXH–NH–CH_3 and GalXMe–NH–CH_3, energy of optimized structures relative to the global minimum energy, population of conformer and the distance between amide proton and the closest oxygen where it can form hydrogen bonds with.

Conformer	Φ (°)	Ψ (°)	ΔE[a] (kcal/mol)	Population[b] (%)	L[c] (Å)			
					NH–O_9	NH–O_{21}	NH–O_{16}	NH–O_{33}
GalXH–NH–CH_3								
A	179.6	67.2	0.00	87.89	2.204	–	–	2.159
B	168.8	167.4	1.61	6.77	2.164	–	–	2.134
C	39.5	63.5	1.76	5.32	–	–	2.142	2.156
D	15.3	179.4	5.00	0.03	–	2.354	–	2.228
GalXMe–NH–CH_3								
A	168.9	80.6	0.00	94.26	2.129	–	–	2.131
B	164.5	180.0	1.77	5.66	2.215	–	–	2.215
C	3.7	63.5	4.42	0.08	–	–	2.114	2.177
D	2.0	172.7	7.10	0.00	–	2.110	–	2.237

[a] The difference in potential energy between the optimized conformer in a local minimum and the most stable conformer in the global minimum. For global minimum $\Delta E = 0$ kcal mol^{-1} and for local minimum $\Delta E > 0$ kcal mol^{-1}.

[b] Calculated based on the potential energy of conformers in mHa (1 mHa = 627503 kcal/mol) according to the Boltzmann's formula describing the ratio of populations of two states i and j: $N_j/N_i = EXP(-(\varepsilon_j-\varepsilon_i)/kT))$, ε – energy of conformer (mHa), kT~1mHa at room temperature.

[c] Calculated distance between amide hydrogen atom (H_{30} for GalXH and H_{26} for GalXMe) and the closest oxygen atom in the vicinity of this hydrogen atom.

indeed amide protons are engaged in local intramolecular NH-acetal hydrogen bonding, which, in consequence, leads next to the discrepancy in theoretical crystalline segmental length of the sebacic acid and GalX segments along the chain to the a further suppression of crystallinity.

To visualize hydrogen bonding formation by amide hydrogens, 4 optimized structures of GalXH–NH–CH_3 are presented in Fig. 6 (the corresponding structures for GalXMe–NH–CH_3 can be found in Figure S1 of the Supporting Information). The hydrogen atoms H_{30} in two of the most stable conformers A and B form a hydrogen bond with oxygen on the neighboring acetal ring O_9 whereas other conformers exist with the opposite carbonyl oxygen O_{16} (conformer C) or the opposite acetal ring O_{21} (conformer D).

The PES analysis for the corresponding esters of both GalX molecules provides additional information. Both types of molecule, the amides (Fig. 5) and the esters (Fig. 7), possess minima located at similar values of the scanned coordinates i.e. dihedral Ψ and Φ, however, the switch between two conformers requires less energy for esters than for amides (rotational barrier is lower for esters). Amide molecules might be stabilized in their minima by the formation of additional interactions; in this case the formerly described intramolecular hydrogen bonds between amide protons and oxygens from acetal rings. It is noteworthy that in both cases, esters and amides, the minima are in the similar positions however in case of GalX amides they are more pronounced. More specifically the population of each conformer for amides is very polarized with the most stable conformer reaching more than 90% population. The same calculation for esters shows that the ratios of conformers is somewhat more balanced, which means that none of the conformers dominates in the sample (see Figure S1b,c and Table S1).

Experimental CP/MAS and simulated ^{13}C NMR spectra. The number of signals in the spectrum, corresponding to the carbons of GalX, depends on the symmetry of the molecule. Generally, multiple backbone carbon signals (2,4,5,7) are detected when the two GalX acetal rings adopt a configuration with a dihedral angle Ψ progressing towards 0° while the spectra become more compact (limited number of signals) when the Ψ value progresses towards 180°. Furthermore, if more conformers contribute, a single signal also will break up in several signals. This effect is related to the diamagnetic anisotropy of carbon nuclei in the antisymmetric molecule [50]. The experimental CP/MAS of the amorphous homopolymers PA5 (GalXH) and PA9 (GalXMe) are presented in Fig. 8a and b and were confronted with simulated spectra for the most stable conformers of the model compounds in Fig. 9a and b.

In the experimental spectrum of the GalXH polymer (PA5) four significant regions can be distinguished (Fig. 8a). The carbonyl region around 171.2 ppm (carbons 1,8), the acetal region around 97–98 ppm (carbons 3,6), a GalX backbone region between 74 and 80 ppm (carbons

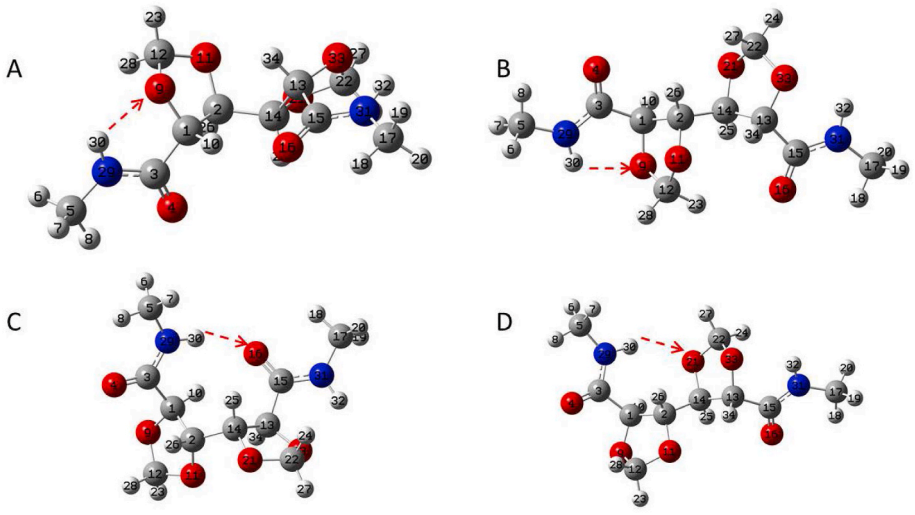

Fig. 6. Optimized structures of conformers A, B, C and D of GalXH–NH–CH_3 and the corresponding intramolecular hydrogen bond formation between hydrogen atom H_{30} and the oxygen atom in its vicinity.

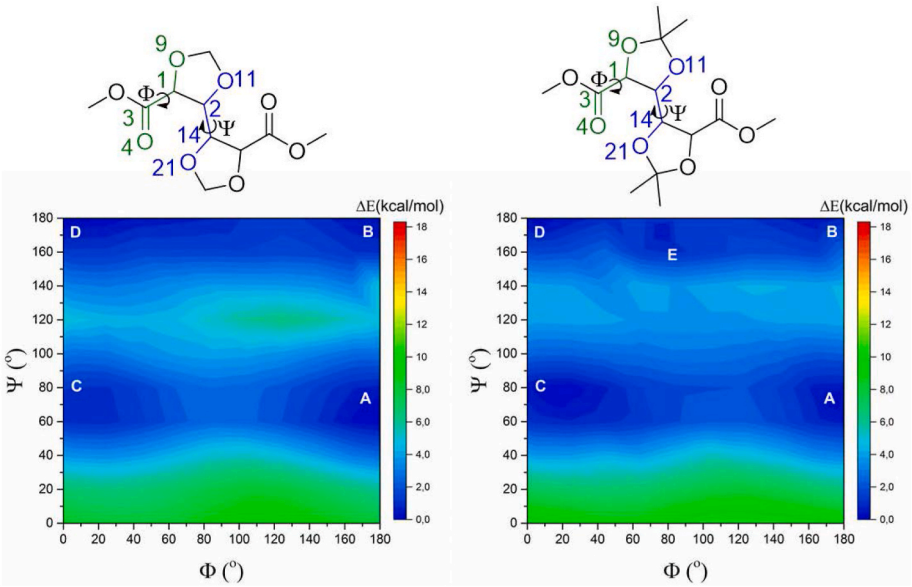

Fig. 7. PES obtained by energy calculation and optimization of two GalX-OCH_3 molecules: GalXH-OCH_3 (left) and GalXMe-OCH_3 (right). The surfaces were calculated along two scanned dihedrals Φ (atoms O_9–C_1–C_3–O_4) and Ψ (atoms O_{11}–C_2–C_{14}–O_{21}) from 0° to 180°. The located minima are labeled as A, B, C, D and E.

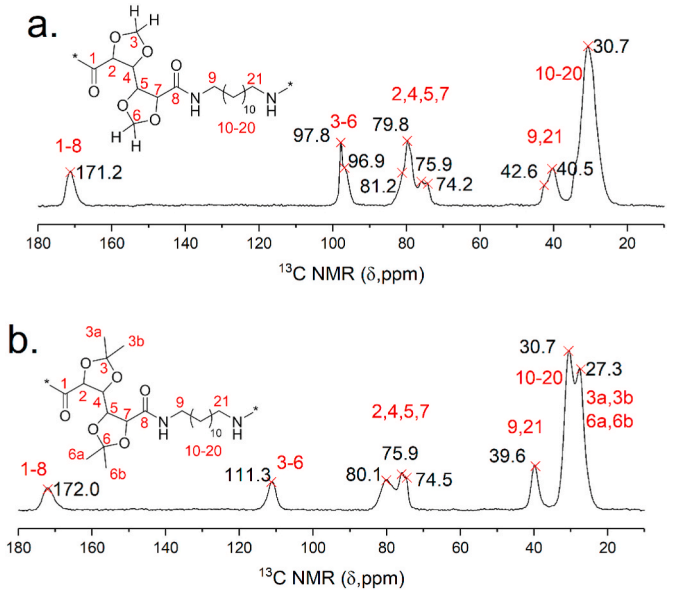

Fig. 8. Solid state CP/MAS ^{13}C NMR spectra of a. GalXH polyamide (PA5) and b. GalXMe polyamide (PA9). *the atom numbering is different for the homopolymers PA5 and PA9, showing only numbers for the carbon atoms, than for the model compounds GalX–NH–CH_3 for which DFT included all atoms of the model compounds.

2, 4, 5, 7) and a region between 39 and 43 ppm arising from methylene carbons connected to a NH group (carbons 9,21). The signals around 30 ppm represent the central methylenes from the DDDA segments. Simulated spectra are presented for three conformers, A, B and C in Table 2 since three of them show populations above 1%. In the experimental spectrum of GalXMe similar regions are visible (Fig. 8b). Simulated spectra are here shown for only two conformers A and B in Table 2 as they have a population above 1%.

The broadening of the carbonyl signals for GalXH and GalXMe (signals around 171–172 ppm) is a first indication for the presence of several possible conformations or alternatively a low mobility of the GalX containing polymeric chains. The region of acetal carbons (3, 6 on Fig. 8a and b) experimentally is around 100 ppm for the GalXH polymer and above 110 ppm for the GalXMe polymer. This is in good correspondence with the simulated spectra shown in Fig. 9. Looking to the experimental spectra, the signal clearly consists of at least two peaks for GalXH whereas a single peak is observed for GalXMe which is just slightly broadened. This confirms that the GalXH polyamide might consist of more conformers than the GalXMe polyamide. The RESULTS confirm the findings of the DFT PES in Fig. 5 showing that GalXH can adopt more stable conformations than GalXMe.

In the experimental spectra, the region of the backbone carbons (carbons 2,4,5,7) is somewhat more extended for the GalXH polymer as compared to the GalXMe polymer: the difference between the peak maxima is 7.0 ppm for GalXH (from 81.2 to 74.2 ppm) while it is only 5.6 ppm for GalXMe (from 80.1 to 74.5 ppm). The width of these regions in simulated spectra are 9.05 and 8.1 ppm for GalXH and GalXMe, respectively. So, also regarding the width of this region, the simulated and experimental spectra show the same trend. Furthermore, the ratio of the signal intensities is different in this region for GalXH as compared to GalXMe: whereas the downfield part dominates for GalXH, the down- and upfield parts have roughly the same intensity for GalXMe. It indicates that the conformer A is dominating in the GalXMe polymer whereas GalXH shows significant contributions of the conformers B and C. This is fully in agreement with the PES images in Fig. 5, which show that the energy barrier between the different conformations is lower for GalXH than for GalXMe, explaining why GalXH can adopt more possible configurations.

The region between 39 and 43 ppm, arising from methylene carbons attached to the NH group of the amide functions, is difficult to confront with the simulated spectra because the DFT simulations were performed for model compounds with a methyl group attached to the NH of the amide instead of a methylene group. Nevertheless, these regions show significant differences between GalXH and GalXMe polymer in experimental spectra. The methylene fragments can adopt two different conformations which can be identified as *trans* (Φ~ 180°) and *gauche* (Φ~60°). This is strongly affected by the γ-gauche effect induced by the γ-substituent [51,52]. In this particular case, this shielding effect by the –NHC═O γ-substituent relates to the mutual H-bonding interactions between acetal oxygen and amide proton (intramolecular) or carbonyl oxygen and amide proton (intermolecular), and thus also influences the chemical shift of the methylene carbon attached to the amide NH group. In other words, different hydrogen bonding interactions are leading to

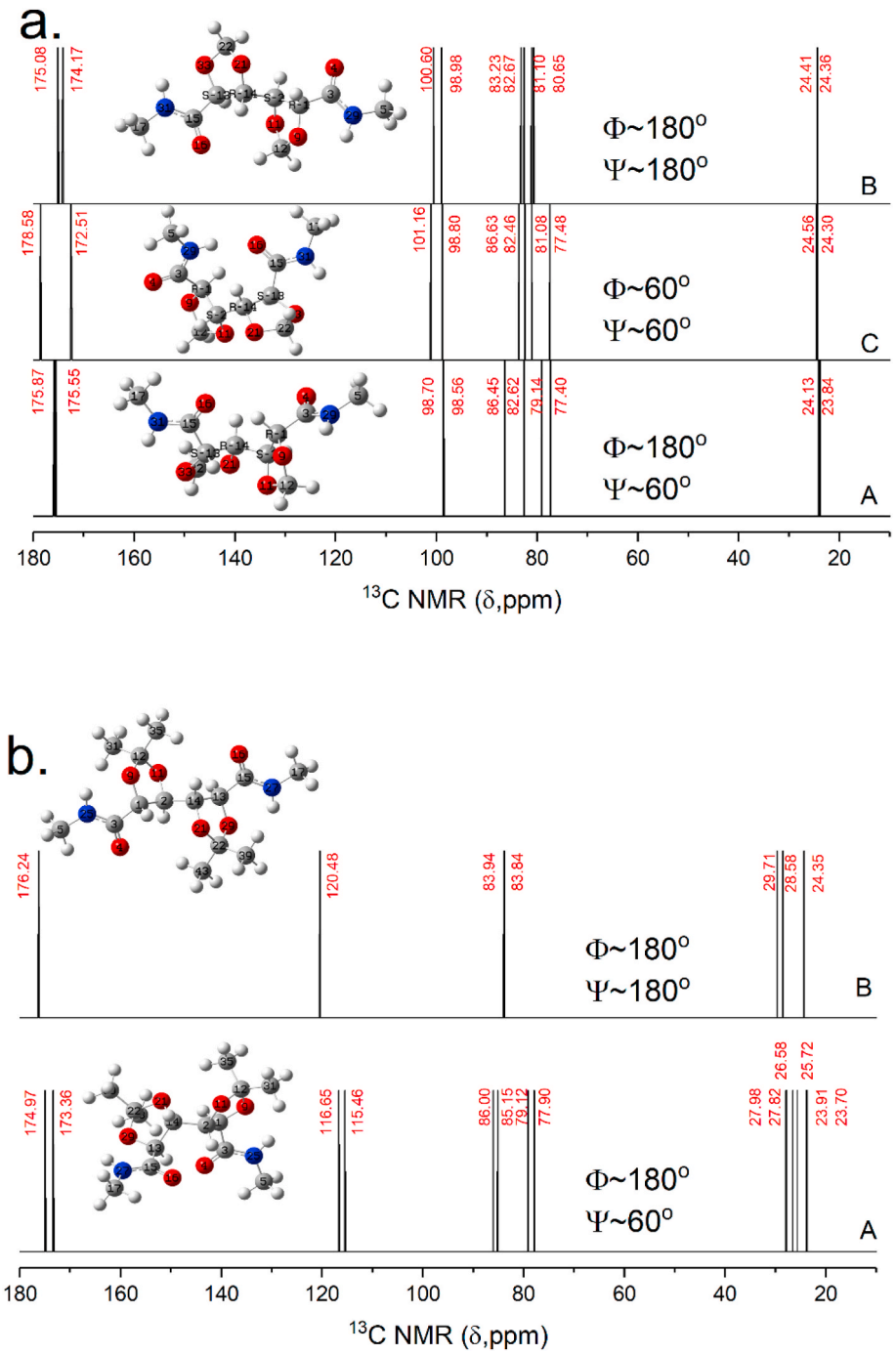

Fig. 9. Simulated spectra of optimized stable conformers of GalX model compounds a. GalXH–NH–CH_3 (conformers A, B, C from Table 2) and b. GalXMe–NH–CH_3 (conformers A, B from Table 2).

gauche and *trans* conformations. In the experimental spectrum of the GalXH polymer two signals can be observed for the methylene unit (40.5 and 42.6 ppm). One presumably corresponds to the *trans* configuration of the methylene fragment while the other represents the *gauche* configuration. On the PES graphs on Fig. 5 we can see that GalXH readily adopts two types of configurations with Φ~60° (conformer C) and Φ~180° (conformers A, B). GalXMe, on the other hand, is prone to adopt the configuration with Φ~180° (conformers A and B) which is in agreement with the higher energy barrier for rotation from *trans* to *gauche* for GalXMe. This indicates that the two species reflected in the spectrum of GalXH by the signals at 40.5 and 42.6 ppm correspond to the *trans* and *gauche* conformations, of which the occurrence is strongly determined by the γ-gauche effect which is different for interchain and intramolecular hydrogen bonding (Fig. 3). For *trans* conformations the intramolecular hydrogen bonds should be dominating while *gauche* conformations demand for interchain hydrogen bonding. It is hypothesized that *gauche* conformer C (Φ~60°) gives a signal at 42.6 ppm while *trans* conformers A and B (Φ~180°), observed for GalXH as well as for GalXMe contribute to the signal around 40 ppm (40.5 ppm for GalXH and 39.6 ppm for GalXMe). In other words, the splitting of the methylene signals can be attributed to the organization of polymer chains in the crystalline domains for GalXH, which is in agreement with DSC data (Fig. 12) showing that GalXH polymers can crystallize from solution whereas no such crystallization was observed for GalXMe polymers.

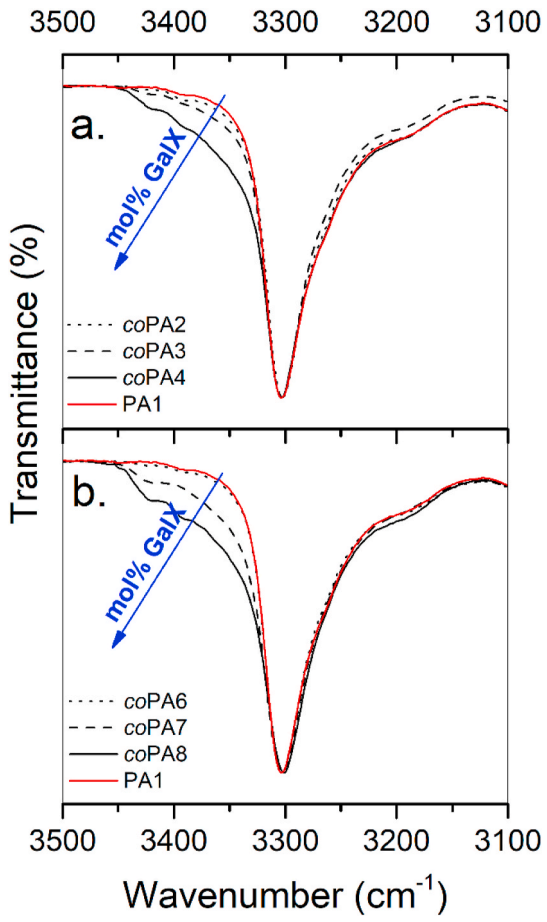

Fig. 10. Representation of the evolution of the hydrogen bonding density (transformation of the N–H stretching vibration) triggered by the introduction of increasing amounts of GalX moieties into homopolyamide PA ($DDDA_{93}$, SA_{100}) (PA1). (a) GalXH copolymer series *co*PA2-*co*PA4 and (b) GalXMe copolymer series *co*PA6-*co*PA9.

Hydrogen bonding efficiency. Investigation of hydrogen bonding in homopolyamides and melting behavior of copolyamides indicates that the cooperative hydrogen bonding efficiency is affected by the increasing concentration of GalX moieties in the polymer (see Fig. 10). The FT-IR spectra recorded for the prepared (co)polyamides PA1, *co*PA2-PA4 and *co*PA6-PA8 show the progressive evolution of the non-hydrogen bonded, broad stretching vibration of N–H. Initially, for the homopolyamide consisting of sebacic acid and 1,12-dodecanediamine (PA1), the peak is sharp and narrow. The visible transformation of the peak occurs above an incorporation of 8–9 mol% GalX into the polyamide structure, at which point the peak starts to broaden because it is affected by a decreasing hydrogen bonding efficiency. The two series of spectra show that the changes are more pronounced for GalXMe (*co*PA5-*co*PA9) and higher concentrations of GalX moieties eventually lead to the existence of a fully resolved additional peak corresponding to non-hydrogen bonded N–H (above 3400 cm^{-1}) already at room temperature. This is a consequence of disrupted packing occurring upon the incorporation of the bulky monomers into polyamide backbones, which is naturally more pronounced for the bulkier GalXMe. We reason that the less N–H protons are actually participating in the interchain hydrogen bonding, the more of them is available for the interactions with acetal oxygen. We already established by DFT calculations that indeed these interactions play a role in the conformations that GalX can adopt. The complete FT-IR characterization of the copolyamides together with temperature dependent FT-IR analysis is available in the Supporting Information Figure S2, Figure S3 and Table S2.

Since the hydrogen bonding in polyamides and resonance structure of the amide group also accounts for the high glass transition temperature in comparison to for example polyesters with identical methylene spacers, the glass transition temperature of the reference polyamide PA (DDDA,SA) and the GalX based copolymers was measured by DMTA. Whereas the conformational rigidity of the GalX moieties leads to an increase in the glass transition upon their copolymerization in polyesters[7,21], Fig. 11 reveals that the glass transition temperature apparent by either the steep decline in storage modulus E' or the maxima in the phase shift tan δ, decreases with an increase in GalX comonomer percentage. The derived glass transition temperatures are summarized in Table 1. Since the glass transition temperature for both the GalH and GalMe copolymers scales identically with increasing GalX comonomer content (Figure S5 in the Supporting Information), it is likely that the suppressed interchain hydrogen bonding lowers the glass transition. It is to be noted that the coPA4 sample upon heating further crystallizes as witnessed by the increase in storage modulus at about 85 °C, Fig. 11a.

Melting behavior. The melting behavior of *(co)*polyamides was studied on films casted from a HFIP solution to facilitate optimum chain packing and to emplify heat flux changes corresponding to the crystalline phase.

Table 1 lists the chemical composition, melting temperatures and crystallinity of all (co)polyamides as collected by DSC. In general, it is widely recognized that crystallinity of a given polymer decreases when (bulky) comonomers are added statistically, because the comonomers are excluded from the crystal. This leaves crystallizable aliphatic chains of shorter and shorter length on increasing the GalX content, explaining decreased crystallinity and T_m [53]. Additionally, aliphatic reference polyamide PA (DDDA,SA) shows a double melting peak of which the first was assigned to reorganization of relatively thin to thicker lamellar crystals upon heating prior to complete melting and the second to an endothermic event [54]. In order to distinguish heat effects of crystallographic reorganizations and true melting, DSC measurements were carried out at a heating rate 1 and 10 °C/min. Independent of the chemical composition, the DSC thermograms recorded at 1 and 10 °C/min reveal that the first endothermic event is less heating rate dependent than the second endothermic event (see Fig. 12a and b).

The small exothermic event that succeeds the first endothermic event, as witnessed at 1 °C/min, supports the reorganization of thin lamellar crystals for both the GalXH and GalXMe copolymers of this study. As a low heating rate provides more time for reorganization, the lamellar thickness of the crystalline phase further increases and so does the melting temperature. Due to the overlapping heat effects, standard DSC cannot be used to evaluate the melting enthalpy and calculate crystallinity accurately. However, two distinct effects are apparent upon the incorporation of GalX comonomers. Firstly, as expected from perturbed chain packing and regardless potential reorganization, increasing the comonomer content decreases the melting temperatures and enthalpies. Secondly, at relatively high comonomer concentration, reorganization prior to eventual melting is no longer observed. This is likely caused by the bulky nature and limited rotational freedom of the GalX comomoners. In fact, especially for the GalXMe copolymers, reorganization is only witnessed at a slow heating rate of 1 °C/min and for the samples *co*PA6 and *co*PA7.

4. Conclusions

FT-IR studies showed that incorporation of GalX motifs into aliphatic polyamides RESULTS in a decrease of the efficiency of hydrogen bonding and corresponding broadening of the N–H amide stretch vibration. This can be related to the fact that GalX amides adopt configurations which allow the formation of intramolecular hydrogen bonds. The GalX esters do not seem to show a similar trend due to the lack of the amide proton that can form the intramolecular hydrogen bond and thus stabilize a particular conformation of the molecule. The hydrogen bonding network that is typical for aliphatic polyamides is disrupted by

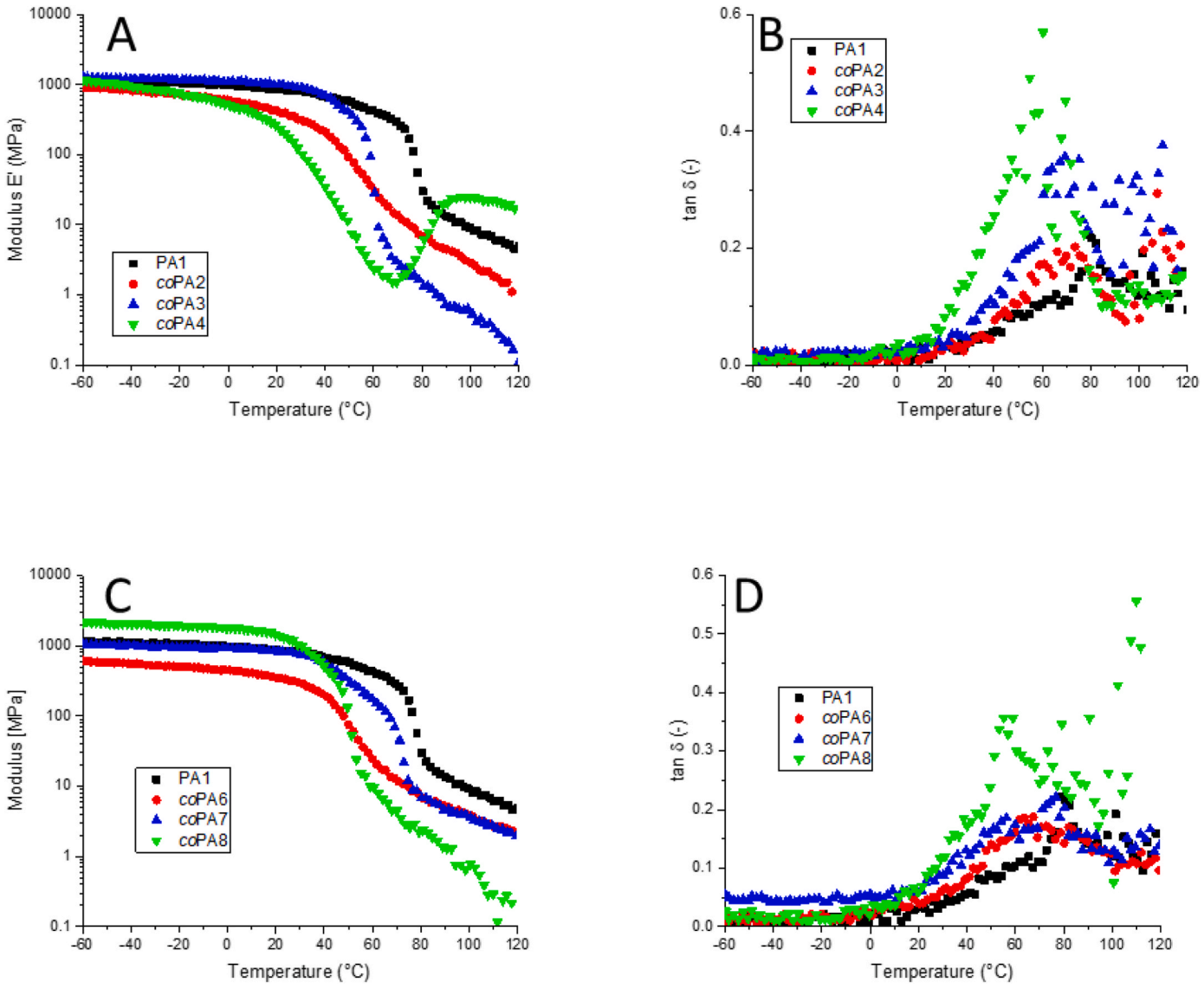

Fig. 11. Dynamic Mechanical Thermal Analysis (DMTA) revealing the storage modulus E′ and phase shift tan δ of the reference polyamide PA (DDDA,SA) (PA1) and the GalXH (a,*b*) and GalXMe (c,d) based copolymers with varying comonomer content.

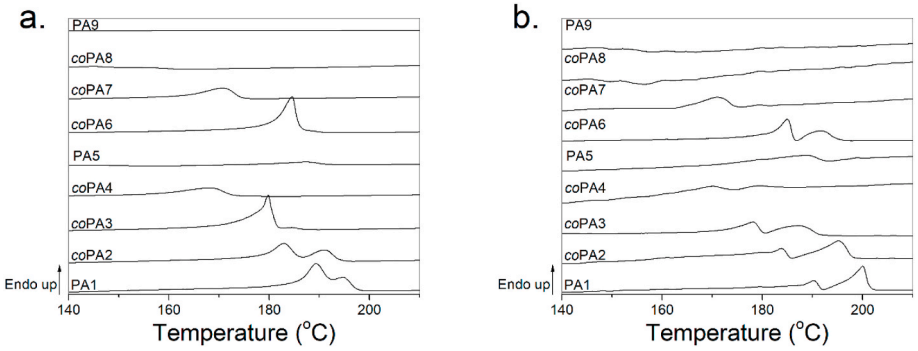

Fig. 12. The melting profiles from the first heating cycle of (co)PA1-(co)PA9 films collected at a heating rate of a. 10 °C/min and b. 1 °C/min.

the presence of the acetal motifs, in particular by the presence of the oxygen on the α carbon which forms an intramolecular hydrogen bond with the neighboring amide proton. Despite the conformational rigidity of the GalX comonomers, the decrease in interchain hydrogen bonding leads to a decrease in glass transition temperature with increasing mole percentage of GalX comonomer. The CP/MAS spectra show that the rotational freedom is higher for GalXH than for GalXMe. The experimental spectra are in agreement with simulated spectra and indicate that the amount of stable conformers which can be adopted is higher for GalXH moieties, as was also proven by calculation of the potential

energy surfaces of GalXH and GalXMe amides.

The incorporation of GalX motifs into copolyamides perturbes the chain packing and leads to a decrease in melting point. The reorganization of thin lamellar crystals upon heating, typically observed above the first melting endotherm, is suppressed due to the rigidity of monomers, especially for GalXMe copolymers. For all copolymers, the melting temperature and enthalpy becomes lower upon increasing the comonomer content.

Funding sources

This work was supported by the "Samenwerkingsverband Noord-Nederland" (SNN; project T3006/Beets to Biopolymers). The authors further acknowledge financial support of Hasselt University and the Research Foundation Flanders (FWO Vlaanderen) via the Hercules project AUHL/15/2 - GOH3816N.

Declaration of competing interest

The authors declare that they have no known competing financial interests or personal relationships that could have appeared to influence the work reported in this paper.

Appendix A. Supplementary data

Supplementary data to this article can be found online at https://doi.org/10.1016/j.polymer.2021.123799.

References

[1] A. Gandini, T.M. Lacerda, From monomers to polymers from renewable resources: recent advances, Prog. Polym. Sci. 48 (2015) 1–39.
[2] C.M. Kshirsagar, R. Anand, An overview of biodiesel extraction from the third generation biomass feedstock: prospects and challenges, Appl. Mech. Mater. 592–594 (2014) 1881–1885.
[3] K. Srirangan, L. Akawib, M. Moo-Younga, C.P. Choua, Towards sustainable production of clean energy carriers from biomass resources, Appl. Energy 100 (2012) 172–186.
[4] B.S. Rajput, S.R. Gaikwad, S.K. Menon, S.H. Chikkali, Sustainable polyacetals from isohexides, Green Chem. 16 (8) (2014) 3810.
[5] C. Lavilla, A. Alla, A.M. de Ilarduya, E. Benito, M.G. Garcia-Martin, J.A. Galbis, S. Muñoz-Guerra, Carbohydrate-based polyesters made from bicyclic acetalized galactaric acid, Biomacromolecules 12 (7) (2011) 2642–2652.
[6] C. Hahn, H. Keul, M. Möller, Hydroxyl-functional polyurethanes and polyesters: synthesis, properties and potential biomedical application, Polym. Int. 61 (7) (2012) 1048–1060.
[7] C. Lavilla, S. Muñoz-Guerra, Sugar-based aromatic copolyesters: a comparative study regarding isosorbide and diacetalized alditols as sustainable comonomers, Green Chem. 15 (1) (2013) 144–151.
[8] S. Amslinger, A. Hirsch, F. Hampel, Synthesis of a biotinated amphiphile, Tetrahedron 60 (50) (2004) 11565–11569.
[9] R. Sablong, R. Duchateau, R. Koelewijn, C.E. Koning, G. de Wit, J. van Haveren, Incorporation of isosorbide into poly(butylene terephthalate) via solid-state polymerization, Biomacromolecules 9 (2008) 3090–3097.
[10] S. Thiyagarajan, L. Gootjes, W. Vogelzang, J. van Haveren, M. Lutz, D.S. van Es, Renewable rigid diamines: efficient, stereospecific synthesis of high purity isohexide diamines, ChemSusChem 4 (12) (2011) 1823–1829.
[11] L. Jasinska-Walc, D. Dudenko, A. Rozanski, S. Thiyagarajan, P. Sowinski, D. van Es, J. Shu, M.R. Hansen, C.E. Koning, Structure and molecular dynamics in renewable polyamides from dideoxy–diamino isohexide, Macromolecules 45 (14) (2012) 5653–5666.
[12] M. Winnacker, B. Rieger, Biobased polyamides: recent advances in basic and applied research, macromol, Rapid Commun 37 (17) (2016) 1391–1413.
[13] Y. Jiang, K. Loos, Enzymatic synthesis of biobased polyesters and polyamides, Polymers 8 (7) (2016) 243.
[14] A.A. Wróblewska, A. Zych, S. Thiyagarajan, D. Dudenko, D. van Es, M.R. Hansen, C. Koning, R. Duchateau, L. Jasinska-Walc, Towards sugar-derived polyamides as environmentally friendly materials, Polym. Chem. 6 (22) (2015) 4133–4143.
[15] A.A. Wróblewska, K.V. Bernaerts, S.M.A. De Wildeman, Rigid, bio-based polyamides from galactaric acid derivatives with elevated glass transition temperatures and their characterization, Polymer 124 (2017) 252–262.
[16] A.A. Wróblewska, S.M.A. De Wildeman, K.V. Bernaerts, In-depth study of the synthesis of polyamides in the melt using biacetal derivatives of galactaric acid, Polym. Degrad. Stabil. 151 (2018) 114–125.
[17] A.A. Wróblewska, J. Noordijk, N. Das, C. Gerards, S.M.A. De Wildeman, K. V. Bernaerts, Structure–property relations in new cyclic galactaric acid derived monomers and polymers therefrom: possibilities and challenges, Macromol. Rapid Commun. 34 (14) (2018) 1800077.
[18] A. Wroblewska, S. Stevens, W. Garsten, S.M.A. Wildeman, K.V. Bernaerts, A solvent-free method for the copolymerization of labile sugar-derived building blocks into polyamides, Sustainable Chem. Eng. 6 (2018) 13504–13517.
[19] M. van Leeuwen, L. Gootjes, W. Vogelzang, R. Knoop, J. van Haveren, D.S. van Es, From Beet Pulp To Building Blocks and Polymers Developing Value Added Materials From GalX. http://edepot.wur.nl/405734. (Accessed 03 October 2017 2017).
[20] M. Metzke, N. O'Connor, S. Maiti, E. Nelson, Z. Gua, Saccharide–peptide hybrid copolymers as biomaterial, Angew. Chem. Int. Ed. 44 (2005) 6529–6533.
[21] E. Zakharova, A. Martínez de Ilarduya, S. Leon, S. Muñoz-Guerra, Sugar-based bicyclic monomers for aliphatic polyesters: a comparative appraisal of acetalized alditols and isosorbide, Des, Monomers Polym 20 (1) (2017) 157–166.
[22] C. Lavilla, A. Alla, A. Martínez de Ilarduya, E. Benito, M.G. García-Martín, J. A. Galbis, S. Muñoz-Guerra, Carbohydrate-based copolyesters made from bicyclic acetalized galactaric acid, J. Polym. Sci., Part A: Polym. Chem. 50 (8) (2012) 1591–1604.
[23] S. Muñoz-Guerra, Carbohydrate-based polyamides and polyesters: an overview illustrated with two selected examples, High Perform. Polym. 24 (1) (2012) 9–23.
[24] P. Ruiz-Donaire, J.J. Bou, S. Muñoz-Guerra, A. Rodriquez-Galan, Hydrolytic degradation of polyamides based on L-tartaric acid and diamines, J. Appl. Polym. Sci. 58 (1995) 41–54.
[25] C. Lavilla, S. Muñoz-Guerra, Biodegradation and hydrolytic degradation of poly (butylene terephthalate) copolyesters containing cyclic sugar units, Polym. Degrad. Stabil. 97 (9) (2012) 1762–1771.
[26] M.E. Rogers, T.E. Long, Synthetic Methods in Step-Growth Polymers, John Wiley & Sons, inc., Hoboken, New Jersey, 2003.
[27] E. Hellmann, J. Malluche, G.P. Hellmann, Condensation kinetics of polyphthalamides. II. Polyesters and diamines, Polym. Eng. Sci. 47 (10) (2007) 1600–1609.
[28] J. Malluche, G.P. Hellmann, M. Hewel, H.-J. Liedloff, The condensation kinetics of polyphthalamides. I. Diamines and diacids or dimethylesters, Polym. Eng. Sci. 47 (10) (2007) 1589–1599.
[29] R. Lazeroms, H. Raaijmaakers, C.E. Koning, A. Papegaaij, A. Urmanova, Bis-Diox (ol)ane Compounds, 2018.
[30] S. Muñoz-Guerra, C. Lavilla, C. Japu, A. Martínez de Ilarduya, Renewable terephthalate polyesters from carbohydrate-based bicyclic monomers, Green Chem. 16 (4) (2014) 1716–1739.
[31] M.K. Dowd, D.E. Kiely, J. Zhang, Monte Carlo-based searching as a tool to study carbohydrate structure, Carbohydr. Res. 346 (9) (2011) 1140–1148.
[32] J.M. Brown, M. Manley-Harris, R.J. Field, D.E. Kiely, An NMR study of the equilibration of d-glucaric acid with lactone forms in aqueous acid solutions, J. Carbohydr. Chem. 26 (8–9) (2007) 455–467.
[33] B.P. Jarman, D.E. Kiely, M. Manley-Harris, B.K. Nicholson, The structures and hydrogen bonding networks in crystals of alkylenediammonium salts of galactaric acid, J. Carbohydr. Chem. 28 (3) (2009) 107–123.
[34] D.E. Kiely, A. Vishwanathan, B.P. Jarman, M. Manley-Harris, Synthesis of poly (galactaramides) from alkylene- and substituted alkylenediammonium galactarates, J. Carbohydr. Chem. 28 (6) (2009) 348–368.
[35] B. Begines, F. Zamora, E. Benito, M. de Gracia García-Martín, J.A. Galbis, Conformationally restricted linear polyurethanes from acetalized sugar-based monomers, J. Polym. Sci., Part A: Polym. Chem. 50 (22) (2012) 4638–4646.
[36] T.-M. Chen, Y.-F. Wang, S. Sakamoto, K. Okada, T. Nakaya, Novel segmented polyurethanes having galactitol analogous groups, Des. Monomers Polym. 1 (4) (1998) 447–465.
[37] C. Rosu, I.I. Negulescu, R. Cueto, R. Laine, W.H. Daly, Synthesis and characterization of complex mixtures consisting of cyclic and linear polyamides from EthylBis-ketal galactarates, J. Macromol. Sci., Part A Pure Appl. Chem. 50 (9) (2013) 940–952.
[38] W.A.P. Black, E.T. Dewar, D. Rutherford, Carbohydrate Derived Polyamides, Secretary of Agriculture, 1965.
[39] K. Butler, D.R. Lawrance, Linear Polyamides, 1956. GB.
[40] J. Wu, L. Jasinska-Walc, D. Dudenko, A. Rozanski, M.R. Hansen, D. van Es, C. E. Koning, An investigation of polyamides based on isoidide-2,5-dimethyleneamine as a green rigid building block with enhanced reactivity, Macromolecules 45 (23) (2012) 9333–9346.
[41] L. Jasinska, M. Villani, J. Wu, D. van Es, E. Klop, S. Rastogi, C.E. Koning, Novel, fully biobased semicrystalline polyamides, Macromolecules 44 (9) (2011) 3458–3466.
[42] T. Van Duong, G. Reekmans, A. Venkatesham, A. Van Aerschot, P. Adriaensens, J. Van Humbeeck, G. Van den Mooter, Spectroscopic investigation of the formation and disruption of hydrogen bonds in pharmaceutical semicrystalline dispersions, Mol. Pharm. 14 (5) (2017) 1726–1741.
[43] N.A. Jones, E.D.T. Atkins, M.J. Hill, Investigation of solution-grown, chain-folded lamellar crystals of the even-even nylons: 6 6, 8 6, 8 8, 10 6, 10 8, 10 10, 12 6, 12 8, 12 10, and 12 12, J. Polym. Sci., Part B: Polym. Phys. 38 (9) (2000) 1209–1221.
[44] C. Alemán, S.E. Galembeck, Intramolecular electronic and hydrogen-bonding interactions in N,N'-Dimethyl-2,3-di-O-methyl-l-tartaramide, J. Org. Chem. 62 (19) (1997) 6562–6567.
[45] L. Jasinska-Walc, M. Villani, D. Dudenko, O. van Asselen, E. Klop, S. Rastogi, M. R. Hansen, C.E. Koning, Local conformation and cocrystallization phenomena in renewable diaminoisoidide-based polyamides studied by FT-IR, solid state NMR, and WAXD, Macromolecules 45 (6) (2012) 2796–2808.
[46] M.J. Frisch, G.W. Trucks, H.B. Schlegel, G.E. Scuseria, M.A. Robb, J.R. Cheeseman, G. Scalmani, V. Barone, B. Mennucci, G.A. Petersson, H. Nakatsuji, M. Caricato,

X. Li, H.P. Hratchian, A.F. Izmaylov, J. Bloino, G. Zheng, J.L. Sonnenberg, M. Hada, M. Ehara, K. Toyota, R. Fukuda, J. Hasegawa, M. Ishida, T. Nakajima, Y. Honda, O. Kitao, H. Nakai, T. Vreven, J.A. Montgomery, J.E. Peralta, F. Ogliaro, M. Bearpark, J.J. Heyd, E. Brothers, K.N. Kudin, V.N. Staroverov, T. Keith, R. Kobayashi, J. Normand, K. Raghavachari, A. Rendell, J.C. Burant, S.S. Iyengar, J. Tomasi, M. Cossi, N. Rega, J.M. Millam, M. Klene, J.E. Knox, J.B. Cross, V. Bakken, C. Adamo, J. Jaramillo, R. Gomperts, R.E. Stratmann, O. Yazyev, A. J. Austin, R. Cammi, C. Pomelli, J.W. Ochterski, R.L. Martin, K. Morokuma, V. G. Zakrzewski, G.A. Voth, P. Salvador, J.J. Dannenberg, S. Dapprich, A.D. Daniels, O. Farkas, J.B. Foresman, J.V. Ortiz, J. Cioslowski, D.J. Fox, Gaussian 09, Gaussian, Inc., Wallingford CT, 2013.

[47] J.B. Foresman, A. Frisch, Exploring Chemistry with Electronic Structure Methods, third ed., Gaussian, Inc., Wallingford, CT USA, 2015.

[48] X. Cui, D. Yan, Crystalline transition of polyamide-10,20 investigated byin situ Fourier transform infrared spectroscopy, J. Polym. Sci., Part B: Polym. Phys. 42 (21) (2004) 4017–4022.

[49] J.A.W. Harings, O. van Asselen, R. Graf, R. Broos, S. Rastogi, The role of superheated water on shielding and mediating hydrogen bonding in N,N′-1,2-Ethanediyl-bis(6-hydroxy-hexanamide) crystallization, Cryst. Growth Des. 8 (9) (2008) 3323–3334.

[50] R.M. Silverstein, F.X. Webster, D.J. Kiemle, Spectrometric Identification of Organic Compounds, seventh ed., John Wiley & Sons, Inc., New York, 2005.

[51] R.K. Harris, NMR studies of solid polymers, in: A.H. Fawcett (Ed.), Polymer Spectroscopy, John Wiley & Sons, Inc., West Sussex (En), 1996.

[52] J. Brisson, J. Gagne, F. Brisse, Model compounds of aromatic nylons. 3. The conformation of the 4T Nylon, poly(tetramethylene terephthalamide), using X-ray diffraction, solid-state ^{13}C NMR spectroscopy and IR spectroscopy, Can. J. Chem. 67 (1989) 840–849.

[53] C. Lavilla, E. Gubbels, A. Martínez de Ilarduya, B.A.J. Noordover, C.E. Koning, S. Muñoz-Guerra, Solid-state modification of PBT with cyclic acetalized galactitol and D-mannitol: influence of composition and chemical microstructure on thermal properties, Macromolecules 46 (11) (2013) 4335–4345.

[54] L. Franco, J. Puiggalí, Structural data and thermal studies on nylon-12,10, J. Polym. Sci., Part B: Polym. Phys. 33 (14) (1995) 2065–2073.